J. Fluid Mech. (1968), *vol.* 33, *part* 4, *pp.* 775–801
Printed in Great Britain

Some electrically driven flows in magnetohydrodynamics Part 2. Theory and experiment

By J. C. R. HUNT
Central Electricity Research Laboratories, Leatherhead, Surrey

AND D. G. MALCOLM†
School of Engineering Science, University of Warwick

(Received 4 July 1967 and in revised form 10 January 1968)

In this part we first extend the theory of part 1 to analyse the distribution of velocity and electric current in an electrically conducting liquid between two circular electrodes of finite diameter, when a current is passed between them. The electrodes are set opposite to each other in insulating planes and a magnetic field is applied perpendicular to these planes. When the Hartmann number $M \gg 1$ we find that the current is confined to the cylinder of fluid joining the electrodes. This effect is accounted for by the velocity which is induced in thin layers of thickness $O(M^{-\frac{1}{2}})$, at the circumference of the cylinder. In our analysis we concentrate on these interesting layers and, amongst other results, we find that in the limit $M \to \infty$ the resistance of the fluid between the electrodes becomes that of the cylinder of fluid joining the electrodes.

We then describe some experiments to test the validity of this theory. In these experiments we measured, as a function of the magnetic field, (*a*) the potential difference between the copper electrodes, the fluid being mercury, (*b*) the electric potential distribution in the fluid between the disks and in the thin layers between the electrode edges, by means of an *electric potential probe*, and (*c*) the velocities induced in the layers using a *Pitot tube*. Our conclusions were: (i) the overall predictions of the theory were correct; (ii) the results of the two probes approximately correlated with each other, despite the theory still having some limitations and the behaviour of these probes still being somewhat uncertain.

1. Introduction

Part 1 of this paper (Hunt & Williams 1968) was an analysis of the flows induced in an electrically conducting fluid by passing current between electrodes placed in non-conducting planes surrounding the fluid, a magnetic field being applied perpendicular to the planes. The analysis was largely concentrated on the interesting physical phenomena which occur when the Hartmann number $M = B_0 a(\sigma/\eta)^{\frac{1}{2}} \gg 1$. ($B_0$ is the applied magnetic flux density, a is a typical length, σ is the fluid's conductivity and η is its viscosity.) The solutions to the problems

† Now at: Department of Mechanical Engineering, University of Saskatchewan, Saskatoon, Canada.

analysed in part 1 demonstrated some of the basic physical effects very clearly and were simple mathematically. However, to contrive those situations *experimentally* proves very difficult, particularly those involving point or line electrodes.

In part 2 we examine the effects of passing an electric current between circular electrodes of finite diameter under the action of a magnetic field, B_0. The geometry of the situation is depicted in figure 1*a*; in this figure is also sketched the pattern of electric current streamlines when $|\mathbf{B}_0| = 0$, the characteristic feature being the spreading of these streamlines. When a magnetic field is applied in the z-direction, i.e. parallel to the direction of current, the $j \times B$ force has, for $z > 0$, a positive component, $(-j_r B_z)$, in the θ or azimuthal direction. A velocity v_θ results, which in turn leads to a reduction in $|j_r|$ because of the induced electric field, $\mathbf{v} \times \mathbf{B}$, being opposed to the original applied electric field. Ultimately a steady flow is created in which the viscous forces, $O(\eta v_\theta/\delta^2)$, are balanced by the $\mathbf{j} \times \mathbf{B}$ forces, $-j_r B_z = O(\delta j_0 B_0/a)$, where δ is the thickness of the layers emanating from the edges. From the curl of Ohm's law, since $\delta \ll a$, $v_\theta = O(j_0 a/\sigma\delta B_0)$, where j_0 is the value of j_z near $r = 0$. Then it follows that $\delta = O(aM^{-\frac{1}{2}})$ and a layer must exist joining the edges of the electrodes through which the electric potential, ϕ, falls and a velocity is induced as shown in figure 1*b*. This effect was first fully appreciated by Moffatt (1964).

In §2 we analyse such a situation, assuming (*a*) that the electrodes are highly conducting relative to the fluid, (*b*) that $M \gg 1$, (*c*) that the fluid is uniform and incompressible, and (*d*) that the radius of the electrodes b is very much greater than δ, the thickness of the layers between the electrode edges, i.e. $b \gg aM^{-\frac{1}{2}}$. From this approximate analysis we obtain some quantitative results and provide a theoretical basis for explaining the results of the experiments. In a forthcoming paper Hunt & Stewartson (1968) deduce a more rigorous asymptotic solution to this problem.

We then describe experiments in which we investigated the effects of a magnetic field on (*a*) the potential difference between the electrodes (copper), (*b*) the potential distribution in the fluid (mercury) between the disks and in the layers between the electrode edges, by means of an electric potential probe, and (*c*) the velocities induced in the layers, using a Pitot tube. These experiments were unlike most MHD experiments in that measurements were made *in* the fluid, as well as at its confining walls. Furthermore, although velocities have recently been measured in MHD flows with Pitot tubes, e.g. Branover & Lielausis (1962) and Moreau (1966), there have been no previous attempts to use Pitot tubes with electric potential probes, to correlate their results, and to compare these results with theory. These experiments are also interesting in that the probe measurements provide a rough check on the theory of MHD probes developed by Hunt (1967).

In §3 the experimental apparatus is described briefly, a more detailed description of the probes and the mechanism for moving the probe being given in appendix A. An outline of the measurement theory of MHD probes is also given there. In §4 the results of the measurements and their interpretation are given and in §5 the main conclusions from the theory and the experiments are presented.

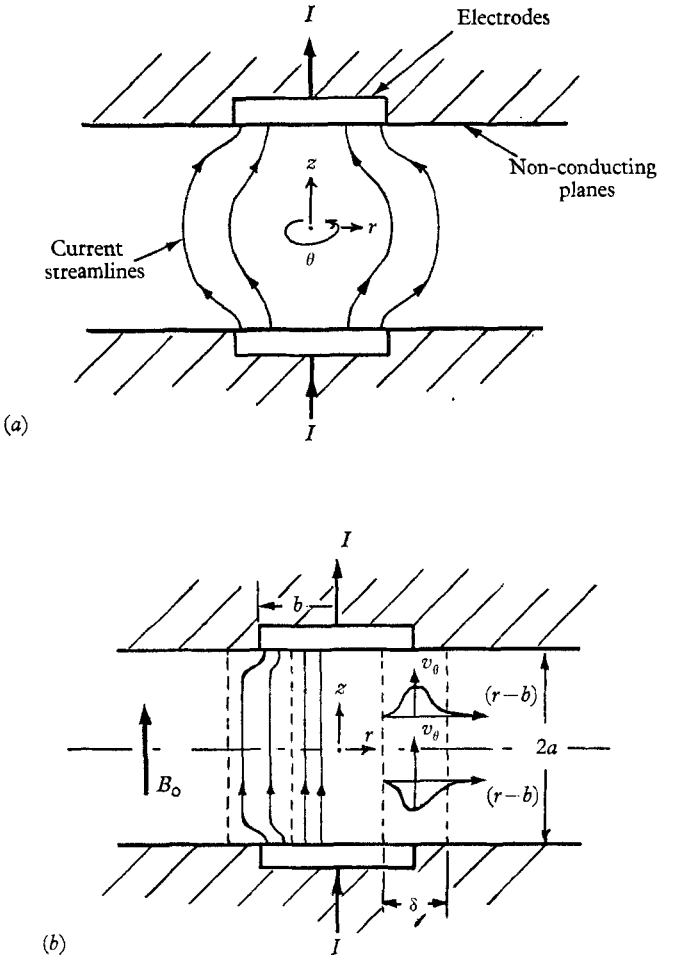

FIGURE 1. Electrically driven flow between circular electrodes. (*a*) Current streamlines when $M = 0$. (*b*) Current streamlines and velocity profiles when $M \gg 1$.

2. Asymptotic analysis of the flow between aligned circular electrodes when $M \gg 1$

In this section we analyse the flow induced by passing a current between two electrically conducting disks (the electrodes) placed opposite each other in non-conducting planes, their surfaces being flush with these planes. A uniform magnetic field of flux density B_0 is applied perpendicular to the planes. (See figure 2.) In our analysis we assume: (i) an incompressible, laminar flow with uniform fluid properties; (ii) a flow in which radial and axial velocities may be ignored (in appendix B we show by theoretical arguments and experimental results that this condition requires $|\mathbf{B}_0|$ to be sufficiently great and the azimuthal velocity, v_θ, sufficiently small); (iii) the boundary conditions and the flow to be axially symmetric; (iv) that $|\mathbf{B}_0|$ is great enough to satisfy the conditions that (*a*) $M^{\frac{1}{2}} \gg 1$,

and (*b*) $M^{\frac{1}{2}}l \gg 1$, where $l = b/a$ is the ratio of the diameter of the electrodes to the distance between them; (v) the electrodes are perfectly conducting.

The first three of these assumptions were made in part 1 of this paper, where

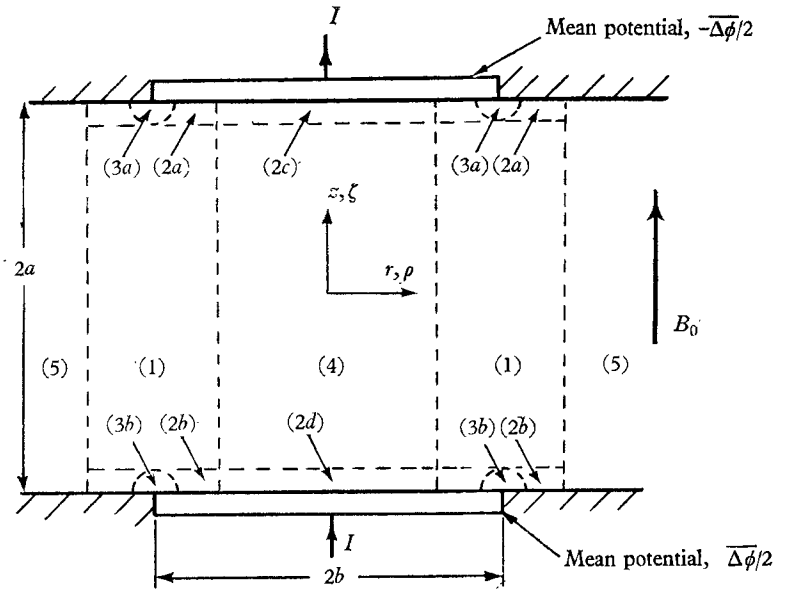

FIGURE 2. Circular electrodes with various regions for asymptotic analysis.

we showed that the relevant equations of MHD in cylindrical co-ordinates may be written in the non-dimensional form

$$0 = M\frac{\partial h}{\partial \zeta} + D_\rho(\rho v) + \frac{\partial^2 v}{\partial \zeta^2}, \tag{2.1}$$

$$0 = M\frac{\partial v}{\partial \zeta} + D_\rho(\rho h) + \frac{\partial^2 h}{\partial \zeta^2}, \tag{2.2}$$

where $$D_\rho = \frac{\partial}{\partial \rho}\left(\frac{1}{\rho}\frac{\partial}{\partial \rho}\right)$$

and $$v = \frac{v_\theta}{I/(2\pi a\sqrt{[\sigma\eta]})}, \quad h = \frac{H_\theta}{I/(2\pi a)}, \quad \rho = r/a, \quad \zeta = z/a,$$

$M = B_0 a(\sigma/\eta)^{\frac{1}{2}}$; I is the total current entering and leaving the electrodes and a is the half distance between them. If we express the electric potential ϕ as the non-dimensional parameter Φ, then $\Phi = \phi/(I/2\pi a\sigma)$ and

$$\partial\Phi/\partial\rho = \partial h/\partial\zeta + Mv, \tag{2.3a}$$

$$\partial\Phi/\partial\zeta = -(\partial h/\partial\rho + h/\rho). \tag{2.3b}$$

We take the potential of the two electrodes as $(-\Delta\phi)/2$ and $\Delta\phi/2$ at $\zeta = \pm 1$, respectively.

As in part 1 we shall be using the composite variable $(v+h)$ for which the governing equation is

$$\frac{M}{\rho}\frac{\partial}{\partial\zeta}(\rho(v+h))+\left(\frac{1}{\rho}\frac{\partial^2}{\partial\zeta^2}+D_\rho\right)\rho(v+h)=0. \tag{2.4}$$

Boundary conditions. On the electrodes and the non-conducting walls at $\zeta = \pm 1$, the first boundary condition is, of course,

$$\mathbf{v} = 0. \tag{2.5}$$

The boundary condition on h at the non-conducting walls ($\rho > l$) is such that $j_z = 0$, whence

$$\text{for} \quad \rho > l, \quad h = 1/\rho \quad \text{at} \quad \zeta = \pm 1. \tag{2.6}$$

On the surface of the perfectly conducting electrodes at $\zeta = \pm 1$,

$$\text{for} \quad \rho < l, \quad \partial\Phi/\partial\rho = \partial h/\partial\zeta = 0. \tag{2.7}$$

If $h = f(\rho)$ on the electrodes we can calculate the value of $f(\rho)$ when $\rho = l$:

$$I = \int_0^b 2\pi r \frac{1}{r}\frac{\partial}{\partial r}(rH_\theta)_{\zeta=\pm 1}\,dr = \frac{Ib}{a}(f(l)-f(0)).$$

If we assume $f(0) = 0$, then

$$f(l) = h(l, \zeta = \pm 1) = 1/l. \tag{2.8}$$

As in part 1, when $M \gg 1$ we divide the space between the boundaries into different regions, as labelled in figure 2, and then analyse these regions in turn.

Region 4. In this region, lying between the electrodes, $\partial/\partial\rho \simeq l^{-1}$ and $\partial/\partial\zeta \simeq 1$, whence as $M \to \infty$ (2.4) becomes

$$M\frac{\partial}{\partial\zeta}(v+h) = 0. \tag{2.9}$$

Then since v is antisymmetric

$$v = \partial h/\partial\zeta = \partial\Phi/\partial\rho = 0.$$

Thence it follows, since the potential is constant on the electrodes, that in region (4)

$$h = \lambda\rho/l^2 \quad \text{and} \quad \Phi = -2\lambda\zeta/l^2, \tag{2.10}$$

where λ is a constant; as it turns out λ is a function of M.

Region 5. In this region, which extends outwards from the edge of the electrodes, the solutions for v and h which satisfy (2.1) and (2.2) and the boundary conditions at $\zeta = \pm 1$, namely (2.5) and (2.6), are:

$$v = 0, \quad h = 1/\rho. \tag{2.11}$$

Matching regions. Now, although the values of h and v for regions (4) and (5) are continuous at $\rho = l$, their derivatives with respect to ρ are not. Therefore the higher derivatives with respect to ρ which were ignored in calculating $(v+h)$ in region (4) become singular and a matching layer must exist. We expect this layer to be of the same form as that analysed in part 1. Therefore we can assume that

the thickness of this layer is $O(M^{-\frac{1}{2}})$ and that, since in this case the current density on the electrode is not specified in regions (2a) and (2b),

$$v+h = f(\rho) = \frac{1}{\rho} + \frac{g(\bar{\rho})}{l^2 M^{\frac{1}{2}}} \quad \text{at} \quad \zeta = \pm 1, \tag{2.12}$$

where $\bar{\rho} = (\rho - l)\, M^{\frac{1}{2}}$ and $g(\bar{\rho})$ satisfies the condition

$$g(\bar{\rho}) = 0 \quad \text{for} \quad \bar{\rho} > 0. \tag{2.13a}$$

In order that regions (1) and (4) should match, $g(\bar{\rho})$ also satisfies the condition

$$g(\bar{\rho}) \to 2\bar{\rho} + \bar{\lambda} \quad \text{as} \quad \bar{\rho} \to -\infty, \tag{2.13b}$$

on making the assumption that

$$\lambda = 1 + \bar{\lambda}/lM^{\frac{1}{2}}. \tag{2.14}$$

Using the same notation and the same approximations as in part 1 for the regions (1), (2) and (3), we find that in region (2a), where $1-\zeta \sim O(M^{-1})$,

$$(v+h)_{(2a)} = f(\rho),$$

and in region (1), where $\bar{\rho} \sim O(1)$ and $\zeta \sim O(1)$,

$$(v+h)_{(1)} = \frac{1}{\rho} + \frac{1}{2l^2 M^{\frac{1}{2}}[\pi(1-\zeta)]^{\frac{1}{2}}} \int_0^\infty g(t) \exp\left(-(t-\bar{\rho})^2/4(1-\zeta)\right) dt. \tag{2.15}$$

In region (2b), the other Hartmann-type boundary layer, for

$$\left.\begin{aligned} \bar{\rho} < 0, \quad (v+h)_{(2b)} &= \frac{1}{\rho} + \frac{g(\bar{\rho})}{l^2 M^{\frac{1}{2}}} e^{-M(1+\zeta)} + \left((v+h)_{(1)} - \frac{1}{\rho}\right)(1 - e^{-M(1+\zeta)}), \\ \bar{\rho} > 0, \quad (v+h)_{(2b)} &= \frac{1}{\rho} + \left((v+h)_{(1)} - \frac{1}{\rho}\right)(1 - e^{-M(1+\zeta)}). \end{aligned}\right\} \tag{2.16}$$

We can obtain some useful information from these very incomplete solutions. First, we can show that, if $f(\rho)$ is a function $\bar{\rho}$ near $\rho = l$, then in region (1) the distribution of Φ, for a given value of ζ, is *similar* for all values of $M \gg 1$. We first calculate v in region (1), using the fact that v is antisymmetric in ζ:

$$v_{(1)} = \frac{1}{4l^2 M^{\frac{1}{2}} \sqrt{\pi}} \left\{ \frac{\int_0^\infty g(t) \exp\left(-(t-\bar{\rho})^2/4(1-\zeta)\right) dt}{(1-\zeta)^{\frac{1}{2}}} - \frac{\int_0^\infty g(t) \exp\left(-(t-\bar{\rho})^2/4(1+\zeta)\right) dt}{(1+\zeta)^{\frac{1}{2}}} \right\}.$$

Thus we see that in region (1) $v = O(M^{-\frac{1}{2}})$. Also, since $\partial h/\partial\zeta = O(M^{-\frac{1}{2}})$ and $Mv = O(M^{\frac{1}{2}})$, it follows that

$$\frac{\partial \Phi}{\partial \rho} = Mv, \tag{2.17}$$

a result peculiar to shear layers like these, which was first noted by Moffatt

(1964). Thence, since $\Phi = 0$ when $\bar{\rho} \to \infty$,

$$\Phi = -\int_{\bar{\rho}}^{\infty} (M^{\frac{1}{2}} v)\, d\bar{\rho}, \tag{2.18}$$

and therefore, in our experiments, if we measure Φ as a function $\bar{\rho}$ at a given value of ζ, we should expect the results to be independent of M.

The second result we can deduce from our approximate analysis is the resistance, R, of the fluid between the electrodes, as $M \to \infty$. Since this result is not dependent on the electrodes being perfectly conducting we define R as

$$R = \overline{\Delta\phi}/I, \tag{2.19}$$

where

$$\overline{\Delta\phi} = -\frac{1}{\pi b^2}\int_0^b \left[\phi(r)\right]_{-a}^{+a} 2\pi r\, dr$$

is the mean value of the potential difference between the disks. From this definition and (2.3) we have

$$R = \frac{2}{\pi\sigma b}\int_{-1}^{+1} (h)_{\rho=l}\, d\zeta. \tag{2.20}$$

Now it follows from our solution (2.15) and the boundary conditions placed on $g(\bar{\rho})$ that

$$\lim_{M\to\infty} (v+h)_1 = \frac{1}{l}, \quad \text{when} \quad \rho = l.$$

Since $(v+h) = O(v+h)_1$ in regions (2) and (3),

$$\int_{-1}^{+1} (v+h)_{\rho=l}\, d\zeta = \int_{-1}^{+1} (v+h)_1 d\zeta + O(M^{-1}), \tag{2.21}$$

and therefore, since v is antisymmetric in ζ, using (2.18),

$$\lim_{M\to\infty} R = R_\infty = \frac{2a}{\pi\sigma b^2}. \tag{2.22}$$

This result does not depend on the function $g(\bar{\rho})$; it depends only on the fact that $g(\bar{\rho}) = 0$ at $\rho = l$. From (2.15) and (2.21), we might expect the next approximation in M, as $M \to \infty$, to be

$$R = R_\infty \left(1 - \frac{k}{lM^{\frac{1}{2}}}\right), \tag{2.23}$$

where k is some constant. Clearly, if the electrodes are highly conducting, $\overline{\Delta\phi} = \Delta\phi$, it follows then that $\overline{\lambda} = -k$, and that in regions (4), as $M \to \infty$,

$$\frac{\phi/I}{a/\pi\sigma b^2} = \frac{\Phi}{2/l^2} = -\zeta(1 - k/lM^{\frac{1}{2}}). \tag{2.24}$$

The physical reason for the dependence of R on $(lM^{\frac{1}{2}})^{-1}$ is that since the thickness of the region (1) is always $O(M^{-\frac{1}{2}})$ the current density in the z direction, for a given value of I, is less by $O(lM^{\frac{1}{2}})^{-1}$ than if there were no 'bulging' of the current lines at all (i.e. the limiting case). This implies that $\partial\phi/\partial z$ and consequently the resistance is also reduced by $O(lM^{\frac{1}{2}})^{-1}$.

3. The experimental apparatus

Our experiments on electrically driven flows using mercury as the conducting fluid were performed in a rectangular duct which had originally been constructed as a prototype for a much larger duct, described by Hunt (1967), and which was then modified for examining electrically driven flows (see figure 3). For the first set of experiments two Perspex blocks, $\frac{1}{2}$ in. thick, were made with copper disks $\frac{3}{4}$ in. in diameter ($= 2b$) and $\frac{1}{4}$ in. thick ($= t$) let into them, the surfaces

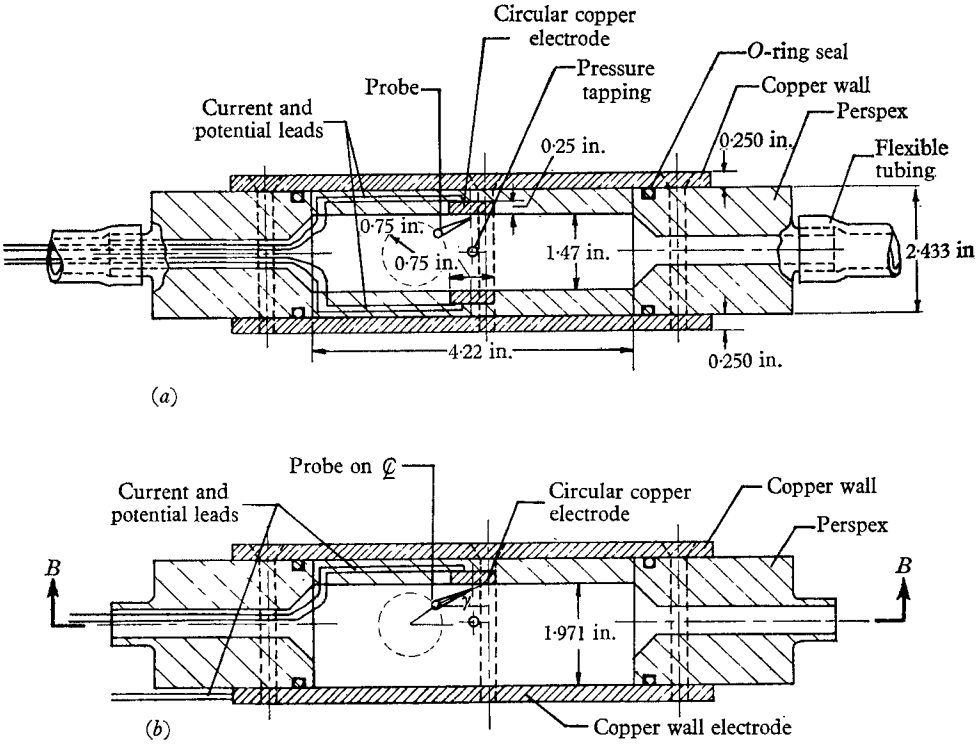

FIGURE 3. Apparatus for examining electrically driven flows. (*a*) Section of the first apparatus. (*b*) Section of the second apparatus. (*c*) Section *BB* through both.

of the copper disks being flush with those of the Perspex blocks (figure 3*a*). The blocks were placed either side of the duct with a gap of 1·47 in. ($= 2a$) between them, so that $l = b/a = 0{\cdot}512$. (The copper side walls of the duct were isolated from its interior by rubber sheets to avoid any short circuits.) Each disk had two wires connected to it, one to supply the current and the other to measure the electrical potential of the disk. A fifth wire was placed in one of the tubes leading out of the duct, its purpose being to measure the potential far away from the electrodes.

We found that, with this first apparatus, the layers emanating from the disk edges were not sufficiently thick compared to the width of the probe. Also, since we were interested in examining the flow at a different value of l, we performed a

second set of experiments in which one of the Perspex blocks and the insulation on one of the duct's copper side walls were removed so that we were effectively examining only one half of the space between two disks. The distance from the disk to the copper face was 1·97 in. ($=a$), and thus $l = b/a = 0{\cdot}190$, as shown in figure 3*b*. In this case we attached two wires to the plate to measure potential and transmit the current.

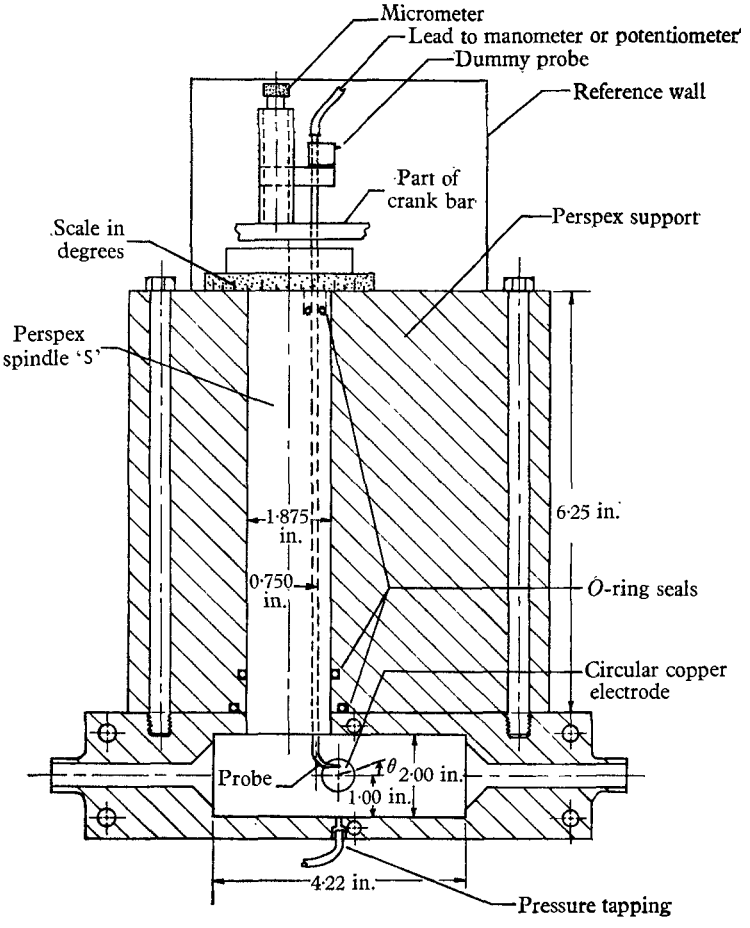

FIGURE 3(*c*). For legend see facing page.

With the duct placed in the electro-magnet in the first apparatus the maximum value of the Hartmann number, M, based on a was about 600 and in the second about 1600. In order that the flows developed were similar to those described in the asymptotic theory of §2, two conditions had to be satisfied by the apparatus. The first was that any error in alignment of the two disks had to be very much less than the thickness of the regions (1); i.e. the layers emanating from the disk edges, which are $O(aM^{-\frac{1}{2}})$, $= O(0{\cdot}030\text{ in.})$. We can confidently say this condition was satisfied by the two disks; with the one disk of the second apparatus this condition did not apply. The second condition was that the thickness of region (1)

should be very much less than the radius of the electrodes, which required that

$$b \gg aM^{-\frac{1}{2}} \quad \text{or} \quad lM^{\frac{1}{2}} \gg 1.$$

The maximum values of $lM^{\frac{1}{2}}$ attainable in the two apparatuses were 13 and 7·7 respectively, which shows that the first apparatus met the conditions of the theory better than the second. (We did not use larger electrodes for fear of the regions (1) touching the top and bottom walls of the duct.) We also note that, if σ_e is the conductivity of the electrodes and t is their thickness, $\sigma a/\sigma_e t$, the relative conductance of the fluid to the electrodes is 0·049 and 0·132 in the two cases.

The object of the experiment was first to measure (by means of a Pye potentiometer) the potential difference between the electrodes when a steady current (measured by an ammeter) was passed between them, as the magnetic field (evaluated from a calibration curve using the measured current in the magnet coils) was varied. The second object was to examine the distribution of the electric potential between the electrodes, which was achieved by the insertion of an

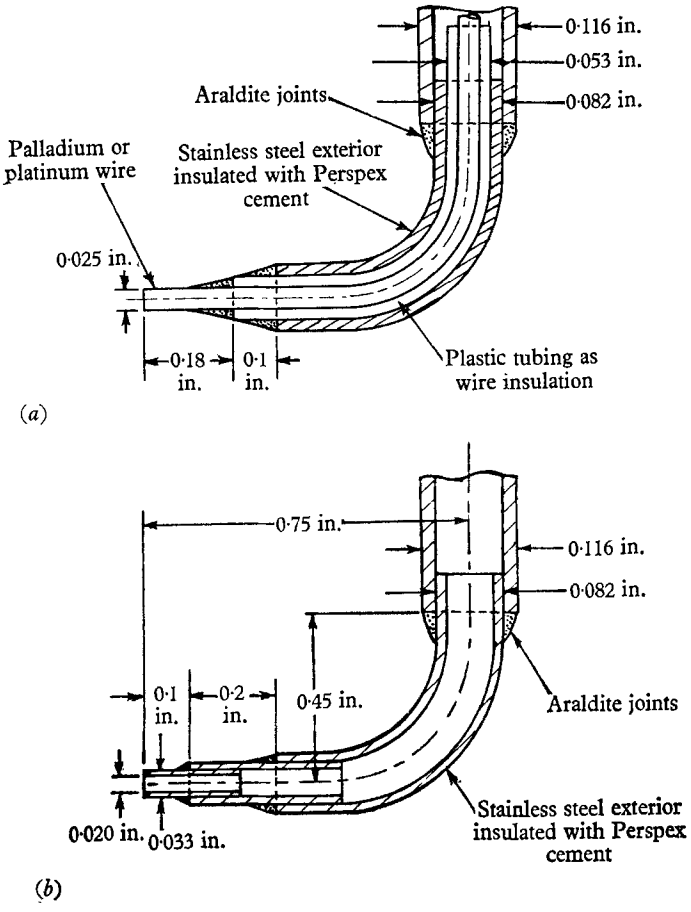

FIGURE 4. Sections through the experimental probes. (*a*) Electric potential probe. (*b*) Pitot tube.

electric potential probe, shown in figure 4*a*, into the fluid and by measuring the difference between the tip of the probe and one of the electrodes, as the probe was moved. The third aim was to examine the velocity in the shear layers existing between the rims of the electrodes by means of measuring the difference in pressure between that at the tip of a Pitot tube, shown in figure 4*b*, and the pressure tapping at the wall, shown in figure 3*c*.

In appendix A these two probes are described along with the mechanism for moving them across the duct.

4. Experimental results

4.1. *Electric potential measurements*

In the first part of the experiment we measured the mean potential difference between the disks, $\overline{\Delta\phi}$, and the difference in electrical potential, ϕ, between the probe and the plane $z = 0$, both as a function of I and M. (In the second apparatus we have calculated $\overline{\Delta\phi}$ by doubling the potential between the electrode and the wall.) In the first instance we wanted to see whether $\overline{\Delta\phi}$ and ϕ were proportional to I at a given value of M, at least for sufficiently small values of I, since all the theory of §2 was based on this assumption. The experimental results shown in figures 5 and 6 show this condition to be well satisfied. These figures also give us some understanding of how the magnetic field affects secondary flows, but this discussion is relegated to appendix B. An important practical point to note in figures 5 and 6 is that the values of $\overline{\Delta\phi}$ and ϕ in the linear regime were always below 100 μV and often below 10 μV. Since the potentiometer only measured to 1 μV and other errors, caused by fluctuations in the magnetic field, temperature effects, etc., were at least of the order of 1 μV, it follows that the errors to be expected were as much as 10% in some places.

Having found the values of I below which it was necessary to operate to avoid the non-linear flow regime, we then measured the variation of R, $= \overline{\Delta\phi}/I$, with M, for the two apparatuses. We showed theoretically in §2 that, whatever the distribution of current density across the electrodes,

$$\lim_{M\to\infty} R = R_\infty = 2a/\pi\sigma b^2.$$

We also demonstrated physically why we could expect R/R_∞ to be a linear function of $(lM^{\frac{1}{2}})^{-1}$ when $M \gg 1$. Therefore, in presenting our experimental results in figure 7 we plot R/R_∞ against $(lM^{\frac{1}{2}})^{-1}$ for the two electrode configurations in which $l = 0{\cdot}512$ and $0{\cdot}190$ respectively. The two main conclusions from these results are first that R/R_∞ is indeed a linear function of M, secondly that, to within the experimental error, the points for the two values of l fall approximately on the same straight line, and thirdly that to within 2% $R/R_\infty = 1{\cdot}00$ when this line is extrapolated to the point where $M = \infty$. It is unfortunate that so few readings were taken for $l = 0{\cdot}190$ because it is hard to tell whether these are falling on a separate curve or are truly scattered about the straight line drawn in figure 7.

Having demonstrated that some of the external characteristics of the

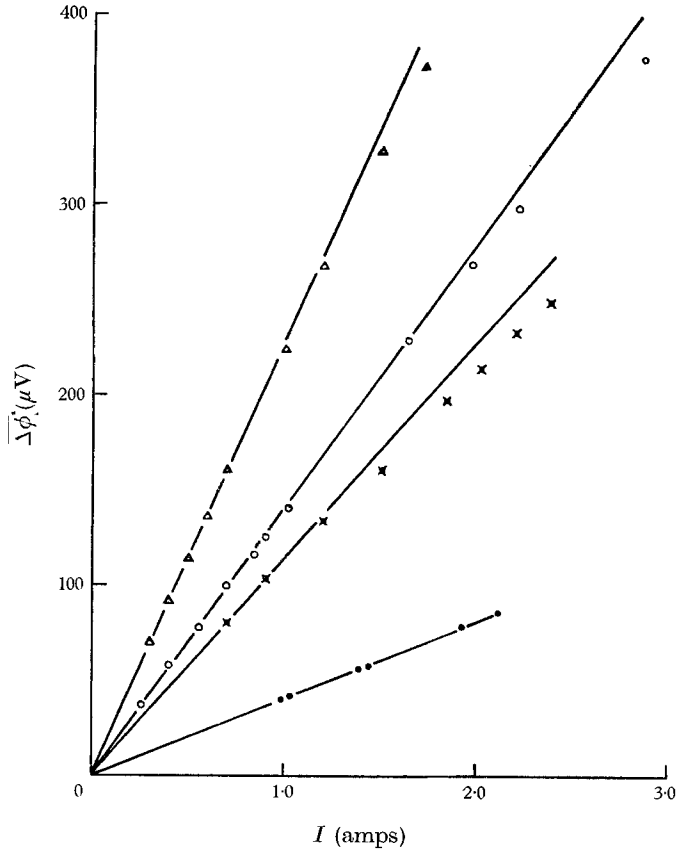

FIGURE 5. Experimental graph of potential between the disks, $\overline{\Delta\phi}$, against current, I, at various values of M. △, $M = 1370$, $l = 0{\cdot}190$; ○, $M = 588$, $l = 0{\cdot}512$; ×, $M = 204$, $l = 0{\cdot}512$; ●, $M = 0$, $l = 0{\cdot}512$.

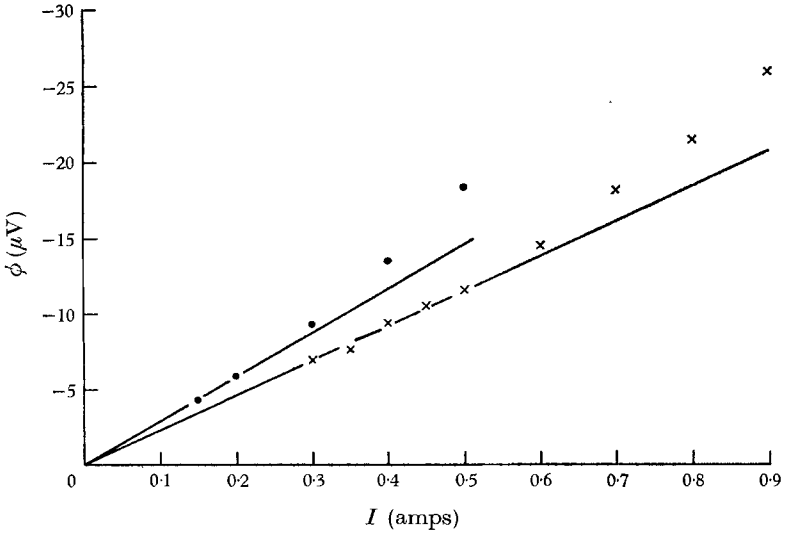

FIGURE 6. Graph of probe potential, ϕ, against I ($l = 0{\cdot}190$; probe positioned at $r/b = 0{\cdot}127$, $\zeta = 0{\cdot}954$). ●, $M = 855$; ×, $M = 1370$.

behaviour were approximately as predicted theoretically, we then examined the internal flow structure. In our theoretical discussion of § 2 we first postulated the existence of various separate regions and then made certain deductions about them, some of which we have been able to verify experimentally. In the central region between the electrodes, region (4), we concluded that when $M \gg 1$ the

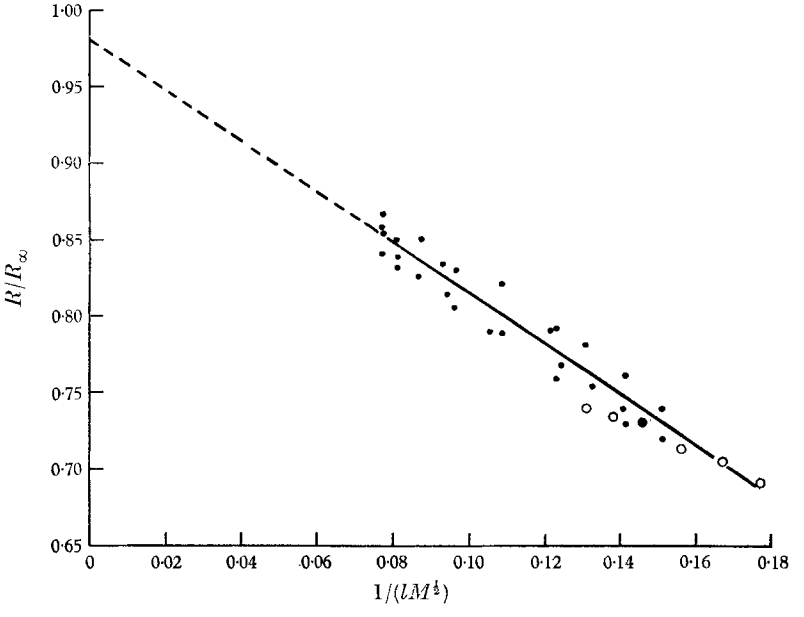

FIGURE 7. Variation of resistance between the electrodes, R/R_∞, with $(1/lM^{\frac{1}{2}})$. ○, $l = 0{\cdot}190$; ●, $l = 0{\cdot}512$.

velocity is zero and that the current density and electric field are uniform, provided the electrodes are perfectly conducting, a condition only approximately satisfied by our apparatus. In figure 8 we have plotted $(-\phi)\sigma\pi b^2/aI$ against ζ along the centre line ($r = 0$) when $M = 0$ and $M \gg 1$, since $(-\phi)\sigma\pi b^2/Ia = \phi/\phi_\infty$, where ϕ_∞ is the value of ϕ on the disk when $M = \infty$ at the same value of I. This figure shows that, when $M = 0$, the current density j_z is lower at $\zeta = 0$ than at $\zeta = 1$ because of the spreading of the current lines, but that, when $M \gg 1$, the current density is the same at all values of ζ, which was predicted by our theory of § 2. Also we conclude that the spreading of the current streamlines is eliminated as shown in figure 1 *b*. The slopes of the two straight lines for two different values of $(lM^{\frac{1}{2}})^{-1}$ are different, as we should expect from the graph of R/R_∞ against $(lM^{\frac{1}{2}})^{-1}$. We should also expect, as indeed we find, that the values of $(-\phi)\sigma\pi b^2/Ia$ are approximately equal to R/R_∞ for these two values of $(lM^{\frac{1}{2}})^{-1}$. We should note that the potential measurements in this region were only likely to be in error to order (d/a), i.e. less than 4 %, owing to MHD effects (see appendix A, equation (A 1)), but the random errors were about 5 %.

We now consider the results of the radial traverses of the electric potential probes in the region (1). Figure 9 shows the results of a potential traverse when $M = 0$,

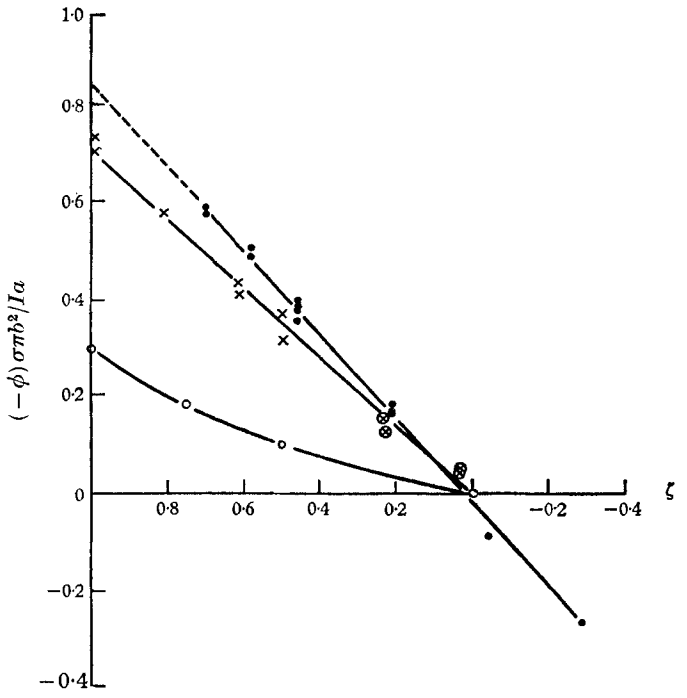

FIGURE 8. Variation of potential, $(-\phi\sigma\pi b^2/Ia)$, along the centre line of the electrodes when $M = 0$ and when $M \gg 1$. ●, $M = 595$, $l = 512$; ○, $M = 0$, $l = 0{\cdot}512$; ×, $M = 1550$, $l = 0{\cdot}190$, $\phi > 0$; ⊗, $M = 1550$, $l = 0{\cdot}190$, $\phi < 0$.

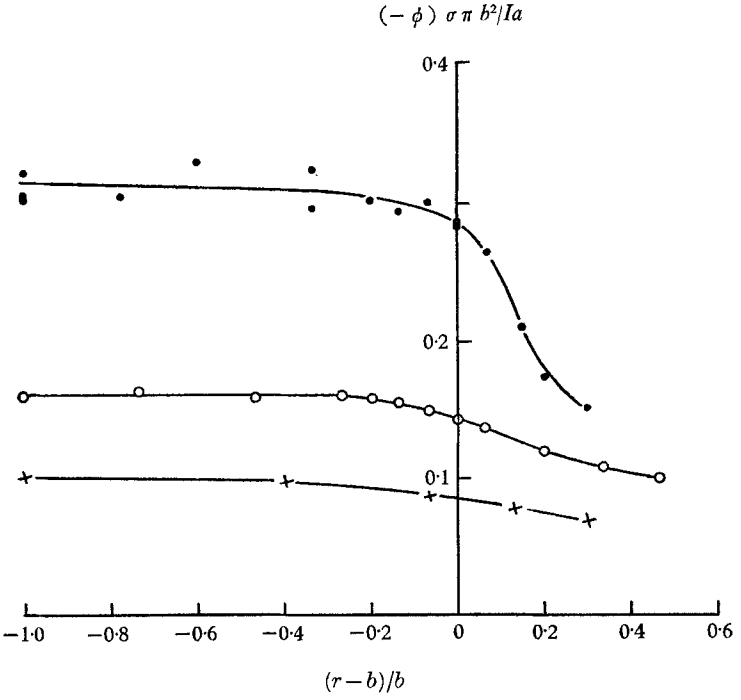

FIGURE 9. Graphs of potential $(-\phi\sigma\pi b^2/Ia)$, against radius, $(r-b)/b$, when $M = 0$. ●, $\zeta = +0{\cdot}97$, $l = 0{\cdot}512$; ○, $\zeta = +0{\cdot}99$, $l = 0{\cdot}190$; ×, $\zeta = +0{\cdot}50$, $l = 0{\cdot}512$.

which acts as a reference with which to compare the results for $M \gg 1$. We made three sets of measurements of ϕ in the first apparatus, i.e. the two disks, when $\rho = 0{\cdot}294$ and $M = 175{,}330$ and 610. (The notation we use is the same as that of figure 2, I being positive when parallel to the magnetic field.) In figure 10*a* we have plotted the results in the form of one graph of $(-\phi)\sigma\pi bl/I$ against $(r-b)/(aM^{-\frac{1}{2}})$ $(=\bar{\rho})$, in order to show firstly that the thickness of the region (1) is unquestionably of order $(aM^{-\frac{1}{2}})$, and secondly to show that the distribution of ϕ and therefore v_θ is similar for different values of M in these layers. We have drawn the best line through the experimental points, because they show only a small systematic departure from this line. Considering the randomness of many of the errors involved, the curves do not indicate any large-scale departure from similarity except where $(r-b)/(aM^{-\frac{1}{2}}) < -3$, when the values of $(-\phi)$ are lower for the lower values of M. This result is to be expected since in the central region, (4), $(-\phi)\sigma\pi b^2/aI$ varies linearly with $M^{-\frac{1}{2}}$, $(-\phi)$ increasing as M increases.

The results shown in figure 10*b* were taken in the second apparatus and were plotted in the same way as those in figure 10*a*. In this case the results were taken with the probe just touching the wall or very close to it, $\zeta > 0{\cdot}96$, and, as the figure shows, there is no detectable difference caused by moving the probe very slightly near the wall. As well as indicating the similarity of the ϕ profiles (in the sense of § 2), these results also show that near the edge of the disk $(-\phi)$ decreases and the distance in which this drop occurs is $O(aM^{-\frac{1}{2}})$. Therefore the electrodes cannot be considered as resembling perfectly conducting electrodes, because, if they were, the probe would have recorded a constant potential across the electrode, at least to within a probe error of $O(d/a)$.

It is interesting that the thickness of the layers are approximately the same in all cases, being about $6aM^{-\frac{1}{2}}$, so that the ratio of the thickness of the layers to the radius of the electrodes is $\delta/b = 6(lM^{\frac{1}{2}})^{-1}$. For the maximum value of M in the first apparatus $\delta/b = 0{\cdot}46$ and in the second apparatus $\delta/b = 0{\cdot}78$. Therefore the approximation we made in § 2 that $\partial/\partial\rho \gg 1/\rho$ is not really justifiable in analysing our experimental situation, and consequently we ought not to expect the degree of agreement that we find for the values of R/R_∞ against $(lM^{\frac{1}{2}})^{-1}$ in the two apparatuses; nor should we expect the ϕ profiles to be the same, even if they had been measured at exactly the same value of ζ.

4.2. *Pitot tube measurements*

As with the electric potential probes, when we began to use the Pitot probe we first checked that we were measuring a velocity *low* enough to be in the required linear flow regime. With the Pitot tube we also had to ensure that the measured velocity was *high* enough for $(p_0 - p_s)$ to be proportional to the square of the velocity v_θ, where p_0 and p_s are the total and static pressure, respectively. Since in the flow regime examined in § 2 v_θ is proportional to I and since it follows from (A 7) that p_0 is proportional to v_θ^2, if the MHD error is small, we had to find the values of I for which $\Delta p = p_0 - p_w$ was proportional to I^2, where p_w is the pressure at the tapping on the wall.

In figure 11*a* we plot Δp against I^2 when $r = 0$, $M = 1370$, and when $r = 1{\cdot}33b$, $M = 855$, these and all subsequent readings being taken in the second apparatus,

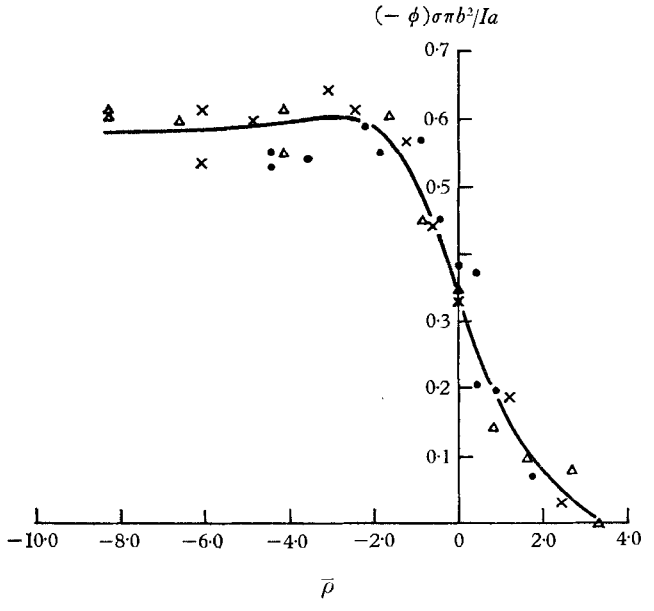

(*a*)

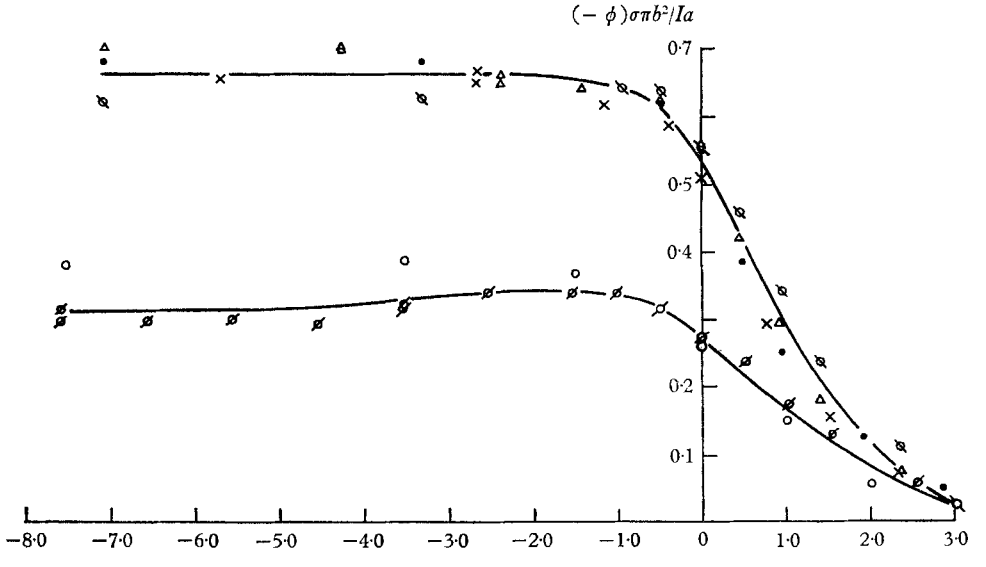

(*b*)

FIGURE 10. Variation of potential with radius in region (1) when M $\gg$ 1. (*a*) $(-\phi\sigma\pi b^2/Ia)$ against $\bar{\rho} = (r-b)/(aM^{-\frac{1}{2}})$; $l = 0{\cdot}502$, $\zeta = 0{\cdot}706$. ●, $M = 175$; ×, $M = 330$; △, $M = 610$. (*b*) $(-\phi\sigma\pi b^2/Ia)$ against $\bar{\rho}$; $l = 0{\cdot}190$. △, $M = 1367$, $\zeta = 0{\cdot}97$; ×, $M = 882$, $\zeta = 0{\cdot}99$; ●, $M = 1367$, $\zeta = 0{\cdot}99$; ○, $M = 1367$, $\zeta = 0{\cdot}96$; ○, $M = 1550$, $\zeta = 0{\cdot}50$; ⌀, $M = 1575$, $\zeta = 0{\cdot}50$.

where $l = 0{\cdot}190$. Note that, when $r = 0$, $\Delta p < 0$ since $v_\theta = 0$ and the static pressure is below the outside the disks due to the radial pressure gradient. When $r = 1{\cdot}33b$, $\Delta p > 0$, showing that in region (1) the rise in total pressure is greater than the fall in static pressure, which is, of course, to be expected.

Realizing that the most critical region for examining the onset of secondary flow was region (1), we then measured Δp at two values of M when $r = 1{\cdot}267b$. The results, plotted in figure 11*b*, show, first, that the velocity decreases as M increases for given I, as is to be expected from the theory of §2, and, secondly, that to operate in the required regime we needed to measure pressures of the order of $-0{\cdot}025$ in. water, which are about as low as can be measured with any degree of repeatability. This meant that we had to operate at high values of M, with the associated disadvantage of using the Pitot tube when the thickness of region (1) was least. We have to presume that, though the MHD probe error for these values of I was about 50 % of the measured value, the random errors preclude any conclusion as to the exact linearity of the Δp *vs.* I^2 relation.

We measured the radial distribution of Δp at $\zeta = 0{\cdot}991$ and $\zeta = 0{\cdot}972$ at only one value of M, 1370, since we could not lower M enough to obtain appreciably different yet repeatable readings and at only one value of I, 0·7 amps. From the radial distribution of Δp we calculated v_θ using the relations (A 9). Since Δp is positive in region (1) and negative in (4) it is zero on the boundary between these two regions and consequently it is impossible to calculate the velocity there at all accurately. We have plotted $v_\theta a l^2 M^{\frac{1}{2}}(\sigma\eta)^{\frac{1}{2}}/I$ against $(r-b)/(aM^{-\frac{1}{2}})$ in figure 12 so that if a suitable theory can be developed it may be compared with these results. We note that the velocity is greatest nearest the wall, which is predictable since the jump in potential across the layer is greatest when ϕ is greatest, i.e. near the disk. Also note that, as *r decreases*, v_θ *decreases* more sharply near the wall, which is to be expected since, if the wall is highly conducting, the current must leave the electrode at right angles, thus reducing the shear stress and consequently the velocity at the wall. We may note that the Hartmann boundary layer here was so thin, 0·001 in., as to be negligible.

4.3. *Discussion*

Having calculated the velocity from the Pitot tube readings, we can now compare these values found with those calculated from the electric potential distribution, using the relation,

$$-\frac{\partial \phi}{\partial r} + v_\theta B_0 = 0. \tag{2.17}$$

Rewriting this in a non-dimensional form we have

$$-\frac{v_\theta M a(\sigma\eta)^{\frac{1}{2}}}{I} = -\sigma a^2 \frac{\partial(\phi/I)}{\partial r}. \tag{4.1}$$

In figure 13 we have plotted $\sigma a^2 \partial(\phi/I)/\partial r$ and $v_\theta Ma(\sigma\eta)^{\frac{1}{2}}/I$ against $(r-b)/(aM^{-\frac{1}{2}})$, using the uncorrected readings of the electric potential and Pitot probe. (With

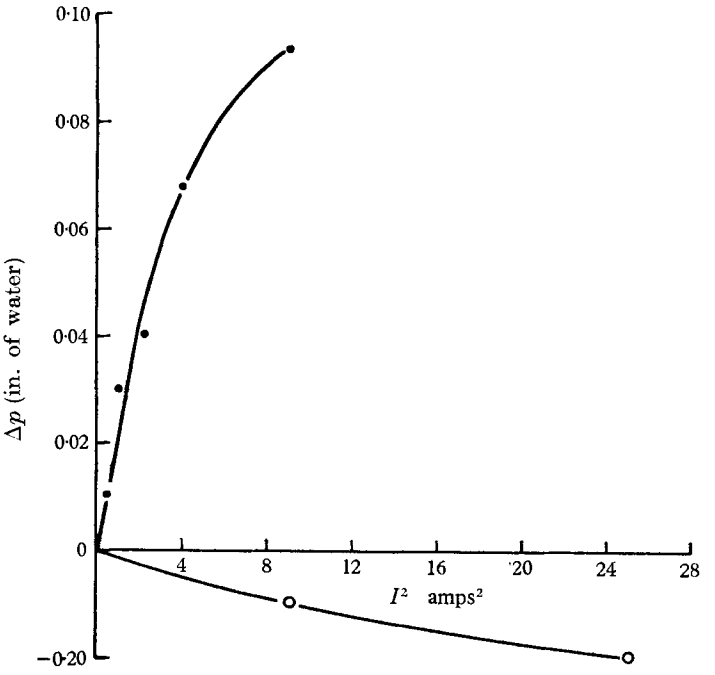

(a)

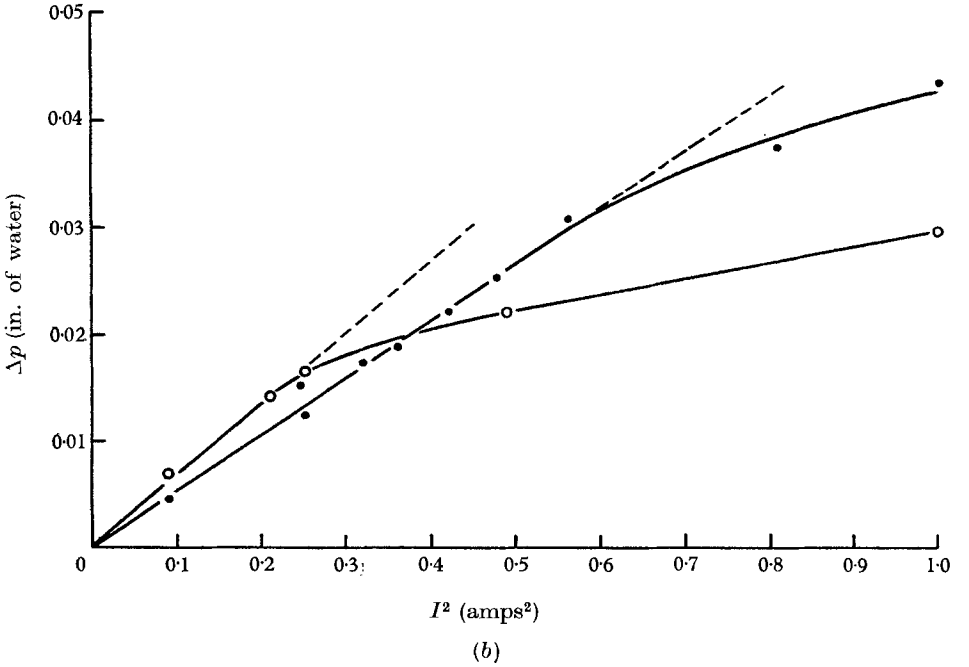

(b)

FIGURE 11. Variation of Pitot pressure, Δp, with I^2 when $M \gg 1$ and $\zeta \simeq -1$. (*a*) Large values of I. ○, $M = 1370$, $r/b = 0$; ●, $M = 855$, $r/b = 1{\cdot}33$. (*b*) Small values of I. ○, $M = 855$, $r/b = 1{\cdot}27$; ●, $M = 1370$, $r/b = 1{\cdot}27$.

the latter we have corrected for the static pressure gradient.) We see that a discrepancy of $>100\,\%$ exists between the two curves. We then calculated $v_\theta Ma(\sigma\eta)^{\frac{1}{2}}/I$ using the correction formula (A 9) (as we did for figure 12), and thence calculated the mean value of $kd^2\partial^2/\partial r^2[Mav_\theta(\sigma\eta)^{\frac{1}{2}}/I]$ across the probe

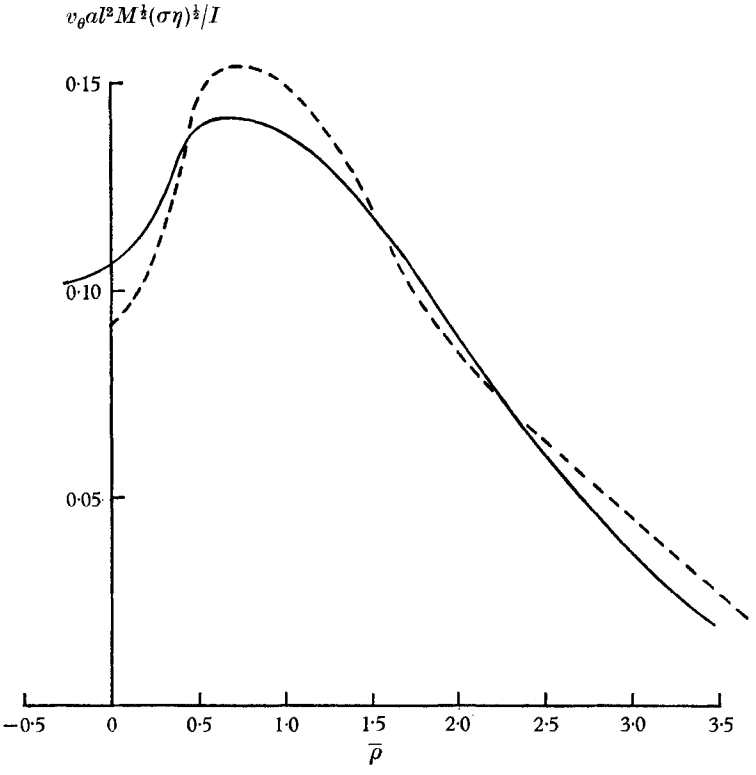

FIGURE 12. Variation of velocity, $v_\theta al^2M^{\frac{1}{2}}(\sigma\eta)^{\frac{1}{2}}/I$, with radius, $\bar{\rho} = (r-b)/(aM^{-\frac{1}{2}})$, in region (1) ($M = 1365$, $I = 0{\cdot}7$ amps). ——, $\zeta = 0{\cdot}97$; — — —, $\zeta = 0{\cdot}99$.

face in order to use the correction formula (A 2) for ϕ_m. (We took $k = \frac{1}{4}$, being the value for the two-dimensional probe examined by Hunt (1967, chapter 4).) We note that, though $d^2M/a^2 \simeq 0{\cdot}1$, since $\partial^2 v_\theta/\partial\bar{\rho}^2$ was so great, the size of the correction term was sufficient to reduce the difference in the maxima to about $30\,\%$. We also note that the maximum of the uncorrected curve of the potential gradient is at a *lower* value of r than the velocity maximum and that, with the correction applied, the maximum moves to a *higher* value of r. We note from figure 13 that this displacement is approximately equal to the diameter of the probe.

The main reason for the difference in these two corrected curves is probably that the experimental situation did not sufficiently satisfy the condition that $\partial/\partial r \gg 1/r$ and that therefore the radial currents were sufficiently large to make (2.17) a poor approximation.

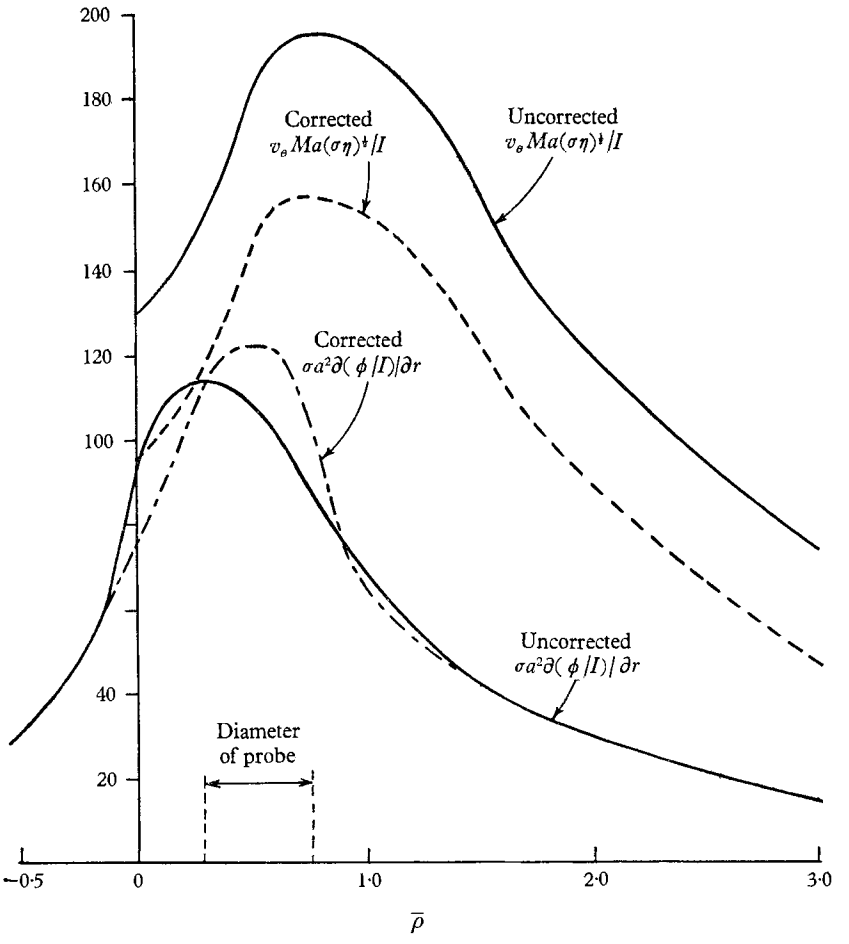

FIGURE 13. Comparison of the values of the velocity calculated from Pitot and electric potential probe readings, both corrected and uncorrected for MHD error ($\zeta = 0{\cdot}991$, $M = 1367$).

5. Conclusions

From our analysis in §2 of the flows induced between two highly conducting circular electrodes we concluded that the following *qualitative* phenomena are to be expected when $M \gg 1$. (i) The 'channelling' of current between the two electrodes. (ii) The existence of a thin layer joining the edges of the circular electrodes in which a large radial electric field and an azimuthal velocity are induced. In this layer the electric field increases and the velocity decreases as M increases. (iii) The variation of the potential distribution across the electrode as M varies, on account of the finite conductivity of the electrode.

Our main *quantitative* predictions are that: (i) If R is the resistance between the two electrodes,

$$\lim_{M\to\infty} R = R_\infty = \frac{2a}{\sigma\pi b^2}, \tag{2.22}$$

whatever the current distribution on the electrodes. From *physical* reasoning we

expect the variation of R with M to be given by

$$R/R_\infty = 1 - k/lM^{\frac{1}{2}}, \tag{2.23}$$

where k is a constant. (ii) If the relative conductance of the fluid to the electrodes is low enough, i.e. if $\sigma a/\sigma_e t \ll 1$, then, provided $(b-r)/(aM^{-\frac{1}{2}}) \gg 1$, $\partial\phi/\partial r = 0$ and $\partial\phi/\partial z$ is constant. (iii) On *physical* grounds we expect the current density distribution to be a function of $\bar{\rho} = (r-b)/(aM^{-\frac{1}{2}})$ on the electrodes. We are then able to conclude mathematically that, if this is so, ϕ is also a function of $\bar{\rho}$ at a given value of z.

It follows that, if the quantitative phenomena (i) to (iii) are shown to exist experimentally, then the qualitative phenomena (i) to (iii) also exist.

In our experiments, described in § 4, we first showed that the relation between R/R_∞ and M took the form of (2.23), whence the result (2.22) follows. We demonstrated that $\partial\phi/\partial r = 0$ and $\partial\phi/\partial z$ is a constant in the region (4), thus confirming the second quantitative prediction, and the first qualitative one. We showed that a thin layer existed between the electrodes' edges and that, in this layer, $\phi\sigma\pi b^2/Ia$ was a function of $\bar{\rho}$, as predicted. In this layer the variation of the velocity with M agreed *qualitatively* with our predictions, though the agreement between the velocity and potential results was not satisfactory. Thus the main conclusions from our physical and mathematical analysis were confirmed experimentally.

The last important result from our experiments comes from the comparison of the results of the Pitot tube and the electric potential probe in an MHD flow and the application of some of the new theory of MHD probes, outlined in appendix A, to explain the differences in their results. (This is the first experiment in which such an exercise has been attempted.) The calculations of velocity in the region (1) deduced from Pitot probe measurements were between 100 % and 400 % higher than those made from electric probe measurements, when no corrections were applied for MHD probe errors. After applying such corrections we found that the differences between the two sets of measurements were reduced to between 30 % and 150 %; also the value of r at the maximum of the electric potential readings became closer to that of the Pitot readings. Thus we conclude that, though our error corrections are of some value, the large discrepancy remaining between the results demonstrates how little we understand the probes. (Some of the discrepancy may be due to the flows not satisfying the conditions of the asymptotic theory, by which we compared the results of the probes.)

We should like to thank Professor J. A. Shercliff for originally suggesting the work on electrically driven flows, and Mr A. E. Webb for constructing the apparatus and endlessly making and changing probes. J.C.R.H. acknowledges the generous support of the Central Electricity Generating Board in supporting this research at the University of Warwick and also acknowledges the support of the U.S. Army Research Office, Durham, North Carolina, at Cornell University, where some of the manuscript of this paper was written. D.G.M. gratefully acknowledges the support provided by the Royal Commission for the Exhibition of 1851 and in part by the National Research Council of Canada, in the form of an Overseas Scholarship.

Appendix A

1. *Electric potential probes*

We mention here a few of the considerations which led to the design of the electric potential probe used in our experiments. On the one hand such a probe needs to be as small as possible, when used in flows such as these where the gradients of velocity and electric potential are large, to avoid the MHD errors discussed by Hunt (1967); the probe size must also be minimized to reduce the size of the vortices shed by the probe which, being carried round, would tend to affect the potential at the probe tip. On the other hand the probe must be sufficiently rigid for its position to be determinate, particularly since in this experiment the probe was not always facing into the flow; also, the conducting region inside the probe must have a sufficient diameter for its resistance to be reasonably low and this wire has to be insulated from the probe's exterior, if this is made of metal.

The fact that the strongest small-diameter tubing easily available is made of stainless steel determined our choice of the material for the probe's exterior. We could either choose to have mercury or a wire inside the probe as our conducting region. The advantage of the wire is that it can be made to protrude from the end of the probe and thus present a small area to the flow. We chose to use palladium and platinum wires, the thermoelectric potential of these wires being close to that of mercury. The final design is shown in figure 4*a*. Note the two diameters of stainless-steel tubing used, the use of flexible plastic tubing as the insulator between the steel tubing and the wire, and the coating of the exterior of the probe with a thin layer of non-conducting Perspex cement.

We now consider the various regions of the flow between the disks, as discussed in §2, in order to estimate the kind of errors to be expected when $M \gg 1$.

Region (4). In this region the current density is uniform and the velocity is zero so that, if the probe is at right angles to the current, i.e. $\gamma = 0$, from the symmetry result of Hunt (1967, chapter 4) no error would be induced. However, as we have explained, the probe could not always be at right angles to the plane $\theta = \frac{1}{2}\pi$, so that we could expect some error due to blocking the currents. Then the error in ϕ compared to $\Delta\phi$ is easily seen to be $O(d/a)$, where d is the probe diameter.

Region (1). In this region severe velocity and potential gradients exist and the equation,

$$-\frac{\partial\phi}{\partial r} + v_\theta B_0 = 0, \tag{2.17}$$

gives the approximate relation between ϕ and v_θ. Now, if the measured potential is ϕ_m and the true potential ϕ, since $\partial\phi/\partial\theta = 0$,

$$\phi_m - \phi = -\int_{-L}^{0} \frac{j_\theta}{\sigma} r\,d\theta - B_0 \int_{-L}^{0} v_r r\,d\theta, \tag{A 1}$$

where L is a large distance, relative to the probe diameter, in the azimuthal direction. (For further discussion of this and other aspects of electric potential probes see Hunt (1967).) Since $N = \sigma B_0^2 d/\rho v_\theta \ll 1$, we can ignore the effect of the magnetic field on the flow over the probe to the first order and then (A 1) becomes

$$\phi_m = \phi + k d^2 B_0 \partial v_\theta/\partial r, \tag{A 2}$$

where k is some positive, dimensionless constant which may be assumed to be independent of v_θ since $R_d = \rho d v_\theta/\eta \gg 1$.

Using (2.17), (A 2) becomes

$$\phi_m = \phi + kd^2\,\partial^2\phi/\partial r^2, \tag{A 3}$$

whence we deduce two results by considering a simple expression to represent the fall of ϕ through the regions (1), say $\phi = 1-\mathrm{erf}(\bar{\rho})$, where $\bar{\rho} = (r-b)/(aM^{-\frac{1}{2}})$. We see that if k is large enough $\partial\phi_m/\partial r$ has two maxima for $\bar{\rho} \lesseqgtr 0$, but that, if k is low enough, the maximum value of $\partial\phi_m/\partial\bar{\rho}$ is *less* than that of $\partial\phi/\partial\bar{\rho}$. To find the condition for the error term to be negligible in region (1), we write (A 3) in terms of $\bar{\rho}$:

$$\phi_m = \phi + \frac{kd^2}{a^2}\,M\,\partial^2\phi/\partial\bar{\rho}^2. \tag{A 4}$$

In our experiments $d^2M/a^2 = 0{\cdot}105$ and therefore we could expect one maximum for $\partial\phi_m/\partial r$ and with a value less than $\partial\phi/\partial r$.

In order to calculate ϕ from ϕ_m we could either integrate (A 4) or, as in fact we did, we could use the results of the Pitot tube readings for v_θ to find ϕ from (A 2). To calculate the error term we averaged the values of $\partial^2\phi/\partial r^2$ or $\partial v_\theta/\partial r$ across the face of the probe, 0·025 in. in diameter.

2. *Pitot tubes*

The considerations leading to the design of the Pitot tube were very similar to those leading to the design of the electric potential probe, the only difference being that the probe should not have too small an internal diameter because of the need to reduce the time for taking a reading of pressure. Again we used various sizes of stainless-steel non-magnetic tubing for the probe, each tube fitting inside the other. The tube was coated with Perspex cement in order to minimize the effects of the probe on the electric fields; however, this was not really necessary as the contact resistance of stainless steel is so large as to render it effectively non-conducting. The final design of Pitot tube is shown in figure 4*b*.

From the theory of Hunt (1967, chapter 4) and the experimental results of East (1964) we expected that the MHD probe errors could be calculated from the formula

$$p_0 = p_s + \tfrac{1}{2}\rho v_\theta^2\left(1+\alpha\frac{\sigma B_0^2 d}{\rho v_\theta}\right), \tag{A 5}$$

where p_0, p_s and ρ are the total pressure, the static pressure and density respectively. It turned out that $N = \sigma B_0^2 d/\rho v_\theta$ was about unity so that higher-order terms in the expansion should have been used. However, the experimental results of East (1964) gave $\alpha = 0{\cdot}39$ and the experimental results of Hunt (1967) gave $\alpha \simeq 0{\cdot}4$ for values of N of $O(1)$, so we assumed $\alpha = 0{\cdot}4$ in our calculations of velocity.

The other source of error to be expected was caused by measuring velocity in a shear flow, i.e. region (1), the length scale of which was somewhat smaller than the diameter of the Pitot tube. However, it was shown experimentally by Hunt (1967) that, if a Pitot tube is used to measure the velocity of a plane Poiseuille

flow in a duct the width of which is only four times that of the tube, the errors over the central half are negligible, but appreciable errors ($\sim 50\,\%$) occur when the centre line of the probe is within one diameter of the wall. However, even that shear flow was less steep than those measured here, so we could expect an appreciable and largely uncertain error in velocity in this highly asymmetric shear flow.

We decided to measure the velocity induced in the region (1) by means of a Pitot tube only, the pressure in the Pitot tube being measured relative to the pressure at a tapping in the wall of the duct, p_w. The static pressure was not measured in the layer, even though there was a small static pressure gradient through the layer caused by the rotating flow. However, this pressure gradient may be calculated from the equation

$$\partial p_s/\partial r = \rho v_\theta^2/r. \tag{A 6}$$

Leaving the error in p_0 for the moment, we have the usual relation between p_0 and p_s, the total and static pressures, i.e.

$$p_0 = p_s + \tfrac{1}{2}\rho v_\theta^2. \tag{A 7}$$

Eliminating p_s from (A 6) and (A 7) we have

$$\frac{\partial p_0}{\partial r} = \frac{\rho v_\theta^2}{r} + \tfrac{1}{2}\rho \frac{\partial v_\theta^2}{\partial r},$$

whence

$$v_\theta^2 = \frac{2}{\rho r^2}\int_\infty^r \left(r^2 \frac{\partial p_0}{\partial r}\right) dr. \tag{A 8}$$

Thus, by only measuring p_0, we could calculate v_θ. Since the static pressure effect is $O(\delta/b)$ ($\ll 1$), we could approximately allow for the MHD error, which was greater than the static pressure effect, by using successive approximations to calculate v_θ, viz.

$$v_{\theta(n)} \simeq 2\int_\infty^r \left(r^2 \frac{\partial p_0}{\partial r}\right) dr \Big/ \left\{\left(1 + \frac{0{\cdot}4\sigma B_0^2 d}{\rho v_{\theta(n-1)}}\right)\rho r^2\right\}. \tag{A 9}$$

(We needed to use two iterations at the most in our calculations.)

3. *The probe mechanism*

To examine the flow between two circular electrodes placed in non-conducting planes opposite each other with a magnetic field parallel to the line joining their centres, we only needed to examine the flow in one plane, $|\theta|$ = constant, because, for low enough velocities, the flow is axisymmetric. Since we wanted to use the mechanism and the probes designed for examining duct flows with the minimum number of alterations, we chose to examine the flows in the plane $\theta = \pm\frac{1}{2}\pi$. As a result of this decision we mounted the mechanism on the duct as shown in figure 3*c*. (This mechanism is similar to that of Lecocq (1964).)

The method of moving the probe in the plane, $\theta = \pm\frac{1}{2}\pi$, may be understood by referring to figure 3*a*, where the locus of the probe stem is shown in the (r, z)-plane ($\theta = 0$). To move the probe tip to a given value of z in the $\theta = \pm\frac{1}{2}\pi$ plane, the probe had to be twisted on its own axis and the probe spindle, S, also twisted.

To move the probe vertically, i.e. to vary r in the $\theta = \pm\frac{1}{2}\pi$ plane, a micrometer screw was used. As a consequence of this method of moving the probes, being $\frac{3}{4}$ in. from their tip to the centre line of their stem, the probes were only able to face into the flow at two positions: (1) $z \simeq +a$, $\zeta \simeq 1$ and (2) in the first apparatus at $z \simeq -a$, $\zeta \simeq -1$, and in the second at $z = 0{\cdot}25a$, $\zeta = 0{\cdot}25$. Therefore, without making new probes of differing lengths, the Pitot tubes could only be used near these values of z, such a probe being accurate to 1 % if it faces into the flow to within 10°. However, the electric probes could be used at all values of z, since they do not critically depend on pointing into the flow, or being at right angles to the current path. But, if γ is the angle between the line joining the probe's tip to the axis of its stem and the duct's axis (see figure 3*a*, *b*), it may be shown from the analysis of Hunt (1967, chapter 4) that the probe errors are reduced if γ is kept to a minimum. When the probe tip was on the duct's centre line, γ took its maximum value, about 45°.

Appendix B. Secondary flow

1. *Orders of magnitude*

As the velocity increases, the form of the flow generated between the electrodes must change in either or both of two basic ways. One possible change is caused by the fact that the azimuthal velocity, v_θ, varies in the radial direction such that $\partial v_\theta/\partial r \gg \partial v_\theta/\partial z$, so that the flow is expected to be unstable somewhat in the manner of a plane jet. Thus, when $v_\theta(aM^{-\frac{1}{2}})\rho/\eta = R_c$, where R_c is the critical value of the Reynolds number of that plane jet which corresponds to the variation of v_θ with r at the highest values of v_θ, we might expect the flow to become unstable to small disturbances, which eventually develop into non-axisymmetric eddies with the major component of the vorticity vector lying in the z direction, i.e. an unsteady flow similar to that found by Lehnert (1956). Since $v_\theta \propto I/M^{\frac{1}{2}}$ from the theory in § 2, it follows that

$$I_c \propto R_c M, \tag{B 1}$$

where I_c is the critical value of I. Thus, for a stable flow at a given value of M, I must be lowered so that $I < I_c$. If the flow becomes unstable in this way, $v_z \neq 0$ and/or $v_r \neq 0$, and in that case the inertial terms would have to be considered in the momentum equation. As a result v_θ, and consequently $\overline{\Delta\phi}$, would no longer be proportional to I.

The second change in the basic flow could be the onset of steady, or unsteady, secondary flow caused by the variation of the azimuthal velocity in the z direction so that $\partial p/\partial r$ $(= \rho v_\theta^2/r)$ varies significantly with z. Thence $v_r \neq 0$, $v_z \neq 0$, and v_θ is changed because the inertial terms in the momentum equation are no longer zero, e.g. $v_z\,\partial v_\theta/\partial z \neq 0$. It is again clear that when this occurs v_θ and $\overline{\Delta\phi}$ are no longer proportional to I.

Thus we conclude that when the basic flow changes, or becomes unstable, we should be able to detect this change by noting the departure from linearity in the variation of $\overline{\Delta\phi}$ with I. Whether a change should become evident at a particular value of I, as in the first instability, or becomes gradually more apparent as in the

gradual onset of a steady secondary flow, cannot be established without a more detailed investigation. Such an investigation of these interesting instability and secondary flow problems has recently been undertaken in which a quartz-insulated hot-film sensor is being used as a flow measurement device in liquid mercury. The results of this investigation will be reported in detail in a forthcoming paper by Malcolm (1968*b*), but one result will be mentioned briefly in § B 2 as it relates to equation (B 1).

2. *Secondary flow measurements*

Figure 5 shows the $\overline{\Delta\phi} - I$ curves for the two apparatuses at various values of M. We note that $\overline{\Delta\phi} \propto I$ when $M = 0$, and that, when $M \neq 0$, the curve of $\overline{\Delta\phi}$ against I is a straight line for I sufficiently small, but as I increases the curve ceases to be a straight line.† From the two curves taken at $M = 588$ and $M = 204$ in the two-disk apparatus ($l = 0{\cdot}512$), we note that the value of I at which the linear regime ceases is higher when M is higher, thus showing that an increased magnetic field tends to suppress the onset of the flow in the non-linear regime. A simple examination of the equations would indicate this result for either of the two non-linear flows discussed in § B 1.

We continued this investigation of the onset of secondary flow by examining the relation between the current, I, and the difference in potential, ϕ, between that on the line $z = 0$ and that measured by the electric potential probe in the one-disk apparatus ($l = 0{\cdot}190$). The probe was placed at a radius of $1{\cdot}27b$ and at a value of $\zeta = -0{\cdot}95$, i.e. in the region (1), so that any secondary flow effects could be markedly demonstrated. As shown in figure 6, the ϕ against I curve becomes non-linear at a much lower value of I for the same value of M than in the $\overline{\Delta\phi}$ against I curve shown in figure 5. The most plausible explanation is that a secondary flow occurs in which the radial velocity tends to thicken the region (1), leading to a reduction at a given value of I of the current density in region (4) and thence $\overline{\Delta\phi}$, as we see in figure 5. However, as region (1) thickens, the potential gradients fall and therefore, if the probe's position is at a radius greater than that of the disk, $|\phi|$ rises, and, if at a lesser radius, $|\phi|$ falls. This explains why, when the curves in figure 6 become non-linear, $|\phi|$ *rises*.

Experimental studies of the stability of the primary flow which are presently under way using the hot-film anemometry technique (Malcolm 1968*a*) indicate that, in the two-disk apparatus ($l = 0{\cdot}512$), the critical current at which the primary flow first becomes unstable varies in the manner, $I_c \propto M$, for $M > 200$. The most interesting consequence of this result is that the critical Reynolds number, R_c, defined in (B 1) must be a *constant* and independent of M, for M sufficiently high. This implies that the magnetic field tends to stabilize the flow chiefly by affecting the primary flow, i.e. lowering its Reynolds number for given I. The other consequence is that, since $v_\theta \propto I/M^{\frac{1}{2}}$, the critical velocity, occurring when $I = I_c$, *increases* as $M^{\frac{1}{2}}$, which agrees qualitatively with the results of figure 11*b*.

† These readings for $M > 0$ were taken to examine the secondary flow, not to measure accurately $\overline{\Delta\phi}/I$ in the primary flow regime. The latter readings were taken later and are not shown.

REFERENCES

BRANOVER, G. G. & LIELAUSIS, O. A. 1962 *Vopr. Magn. Gidro. Akad. Nauk. Latv. SSR., Riga*, **2**, 575–81.

EAST, D. 1964 The Pitot tube in magnetohydrodynamics. Ph.D. Thesis, Mass. Inst. Tech.

HUNT, J. C. R. 1967 Some aspects of magnetohydrodynamics. Ph.D. Thesis, Cambridge University.

HUNT, J. C. R. & STEWARTSON, K. 1968 To be published.

HUNT, J. C. R. & WILLIAMS, W. E. 1968 *J. Fluid Mech.* **31**, 705.

LECOCQ, P. 1964 Contribution à l'étude des pertes de charge et profils de vitesse en écoulement turbulent en magnéto-hydrodynamique. Ph.D. Thesis, Toulouse.

LEHNERT, B. 1956 *Proc. Roy. Soc.* A **233**, 299.

MALCOLM, D. G. 1968*a* Thermo-anemometry in magnetohydrodynamics. Ph.D. Thesis, University of Warwick.

MALCOLM, D. G. 1968*b* To be presented at the 6th Symposium of Magnetohydrodynamics, Inst. of Physics, Acad. of Sciences, Riga, Latvian SSR, Sept. 3–6.

MOFFATT, H. K. 1964 *Proc. 11th Int. Cong. Appl. Mech., Munich*, p. 946.

MOREAU, R. 1966 *C. R. Acad. Sci.* **262**, 259.